In order to connect the coefficient $X(N)$ (in the case $B \neq 0$) to the absorption coefficients $(1-\rho_N^2)^{1/2}$ of the incoming waves, it is necessary to know also the coefficients $X(N)$ connected with the reactions $\pi^- p \to \pi^- p \pi^0$ and $\pi^- p \to \pi^0 \pi^0 n$. Thus, only when measurements in these channels become available will it be possible to determine the absorption coefficients by the study of the inelastic channels.

ACKNOWLEDGMENTS

We are very thankful to Dr. G. Valladas, Dr. B. Deler, and Dr. J. P. Merlo for fruitful discussions.

PHYSICAL REVIEW VOLUME 166, NUMBER 5 25 FEBRUARY 1968

Pion, Kaon, and Antiproton Production in the Center-of-Mass in High-Energy Proton-Proton Collisions*

L. G. RATNER
Particle Accelerator Division, Argonne National Laboratory, Argonne, Illinois

AND

K. W. EDWARDS†
Department of Physics, University of Iowa, Iowa City, Iowa

AND

C. W. AKERLOF, D. G. CRABB, J. L. DAY, A. D. KRISCH, AND M. T. LIN
Randall Laboratory of Physics, University of Michigan, Ann Arbor, Michigan

(Received 11 September 1967)

The differential production cross section $d^2\sigma/d\Omega dP$ has been measured for pions, kaons, and antiprotons produced in 12.5-GeV/c proton-proton collisions. In this experiment we studied the dependence of $d^2\sigma/d\Omega dP$ on the longitudinal and transverse components of the c.m. momenta of the produced particles, P_l and $P_\perp$, while holding all other variables fixed in the center-of-mass system. The ranges of the components measured were $P_l = 0.0$–1.0 GeV/c and $P_\perp^2 = 0.1$–1.5 (GeV/c)^2. The 12.5-GeV/c extracted proton beam of the Argonne ZGS impinged upon a liquid-hydrogen target. The produced particles were detected by a spectrometer containing two bending magnets and Čerenkov counters and scintillation counters in coincidence. The incident proton flux was determined by monitor scintillators calibrated during gold-foil irradiations. The cross sections for the production of $\pi^\pm$ and $K^\pm$ were all found to have an unambiguous Gaussian dependence on $P_\perp$ over the entire range. In the formula $d^2\sigma/d\Omega dP = B \exp(-AP_\perp^2)$, we found $A \approx 3.5$ (GeV/c)$^{-2}$ for $\pi^\pm$ and K^-. However, for K^+ we found $A \approx 2.7$ (GeV/c)$^{-2}$. In studying the dependence of $d^2\sigma/d\Omega dP$ on P_l, we found that the cross section was very strongly peaked about $P_l \approx 0.5$ GeV/c, with very few particles produced near $P_l = 0$. This shows that there is no tendency for particles to be produced at rest in the center-of-mass system. (Such production is predicted by the statistical model.) Instead, particles come out in two clouds or "fireballs" following the two departing baryons. These fireballs have a mass of about 2100 MeV.

1. INTRODUCTION

DURING the past few years there have been several "beam survey" experiments[1–5] performed at high-energy accelerators. In this type of experiment the differential production cross section $d^2\sigma/d\Omega dP$ for the production of secondary particles in high-energy proton-nucleus or proton-proton collisions was measured. These experiments were all done in the laboratory system, in that a series of measurements was made with θ_{lab} held fixed while P_{lab} was varied. The main purpose of these experiments was to obtain information to aid in the design of secondary particles. There were few serious attempts to relate these experimental data to the theory of strong interactions. The reason for the lack of theoretical interest in experiments of this type was that all these measurements were made in the laboratory system while it seems likely that any sensible theory of particle production in strong interactions will be simple only in the center-of-mass system.

* Supported by a research grant from the U. S. Atomic Energy Commission.

† Present address: Department of Physics, Carleton University, Ottawa, Canada.

[1] W. F. Baker, R. L. Cool, E. W. Jenkins, T. F. Kycia, S. J. Lindenbaum, W. A. Love, D. Luers, J. A. Niederer, S. Ozaki, A. L. Read, J. J. Russell, and L. C. L. Yuan, Phys. Rev. Letters **7**, 101 (1961).

[2] A. N. Diddens, W. Galbraith, E. Lillethun, G. Manning, A. G. Parham, A. E. Taylor, T. G. Walker, and A. M. Wetherell, Nuovo Cimento **31**, 961 (1964).

[3] D. Dekkers, J. A. Geibel, R. Mermod, G. Weber, T. R. Willitts, K. Winter, B. Jordan, M. Vivargent, N. M. King, and E. J. N. Wilson, Phys. Rev. **137**, B962 (1965).

[4] R. A. Lundy, T. B. Novey, D. D. Yovanovitch, and V. L. Telegdi, Phys. Rev. Letters **14**, 504 (1965).

[5] E. W. Anderson, E. J. Bleser, G. B. Collins, T. Fujii, J. Menes, F. Turkot, R. A. Carrigan, R. M. Edelstein, N. C. Hien, T. J. McMahon, and I. Nadelhaft, Phys. Rev. Letters **16**, 855 (1966); **19**, 198 (1967).

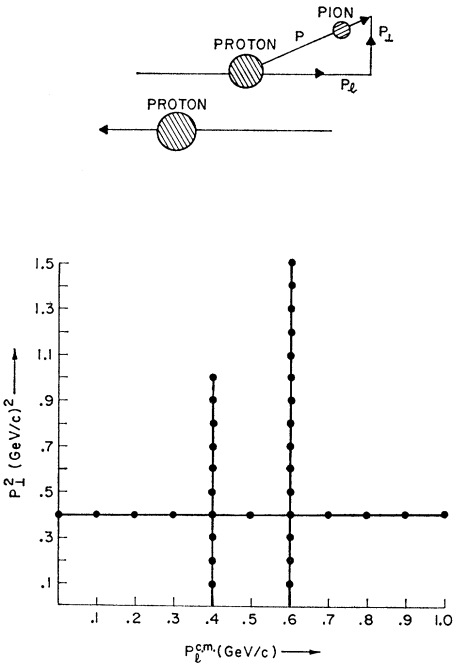

FIG. 1. Plot showing P_l and $P_\perp^2$, the two components of the momentum of the produced particles in the center-of-mass system. The lines drawn indicate the lines along which measurements were made. By symmetry we obtain the cross section in the other three quadrants.

From the existing data, it was impossible to get a unique dependence of $d^2\sigma/d\Omega dP$ on center-of-mass variables although several authors have tried.[5–8]

In this experiment[9] we have measured the differential production cross section $d^2\sigma/d\Omega dP$ for the production of pions, kaons, and antiprotons in high-energy proton-proton collisions. This experiment was done in the center-of-mass system, in the sense that a series of measurements was made varying $P_\perp^2$, the transverse momentum squared of the produced particle in the c.m. system, while holding P_l, the particle's c.m. longitudinal momentum, fixed. Another series of measurements was made with $P_\perp^2$ fixed while P_l was varied. The range covered is shown in Fig. 1 where we have plotted P_l versus $P_\perp^2$. These measurements allowed us to study independently the dependence of $d^2\sigma/d\Omega dP$ on P_l and $P_\perp^2$ in the center-of-mass system.

This experiment was first suggested by a recent 90° proton-proton elastic scattering experiment[10,11] which showed evidence for three regions in proton-proton interactions. It has been speculated by one of us[12] that these three regions are due to the diffraction scattering associated with pion, kaon, and antiproton production. More recently, this idea has been pursued by others.[11,13] The present experiment was designed to search for any connection between the three regions and π, K, and $\bar{p}$ production.

More generally, this experiment serves as an initial attempt to study systematically the dependence of $d^2\sigma/d\Omega dP$ on center-of-mass variables. This dependence is likely to play a central role in the study of the dynamics of strong interactions at high energies.

In Sec. 2 we describe the experimental methods and techniques employed in this measurement. In Sec. 3 we calculate and tabulate the results, while in Sec. 4 a discussion of the results is presented.

2. EXPERIMENTAL METHOD

The layout of the experiment is shown in Fig. 2. The slow extracted beam of the ZGS impinged upon a 2-in.-diam. liquid-hydrogen target and the particles produced in the interaction were detected by a single-arm spectrometer. The spectrometer was adjusted to accept only those particles produced with a particular value of P_l and $P_\perp^2$ in the c.m. system. As we varied the values of P_l and $P_\perp^2$ the c.m. production angle changed, causing a corresponding change in the laboratory angle. The C magnet was set to compensate for this change in laboratory angle. The B magnet deflected the produced particles for momentum analysis.

The number and nature of the produced particles were determined by counting coincidences between the various sets of counters in the spectrometer. The number of protons hitting the H_2 target was determined by two sets of monitor counters. These monitors were calibrated by foil irradiation experiments.

A. Proton Beam

The proton beam was extracted from the ZGS using the Piccioni extraction system containing an energy-loss target which moved the beam into the extraction magnets. The extraction efficiency was about 25%. Between 1 and 2×10^{11} protons of 12.5 GeV/c were extracted during a spill of 300 msec. The ZGS repetition rate was about one pulse every 2.5 sec. The angular divergence of the extracted beam was about ±3 mrad and the momentum spread was less than $\frac{1}{2}$%. The beam spot at the target was a circle of 1-cm diameter. The

[6] G. Cocconi, L. J. Koester, and D. H. Perkins, University of California Radiation Laboratory Report No. UCRL-10022, 1961 (unpublished).
[7] J. Ranft, CERN Report No. MPS/EP 66-4, 1966 (unpublished).
[8] G. H. Trilling, University of California Radiation Laboratory Report No. UCRL-16830, 1966 (unpublished).
[9] L. G. Ratner, K. W. Edwards, C. W. Akerlof, D. G. Crabb, J. L. Day, A. D. Krisch, and M. T. Lin, Phys. Rev. Letters **18**, 1218 (1967).
[10] C. W. Akerlof, R. H. Hieber, A. D. Krisch, K. W. Edwards, L. G. Ratner, and K. Ruddick, Phys. Rev. Letters **17**, 1105 (1966); Phys. Rev. **159**, 1138 (1967).
[11] The existence of these regions has recently been confirmed by J. V. Allaby, G. Cocconi, A. N. Diddens, A. Klovning, G. Matthiae, E. J. Sacharidis, and A. M. Wetherell, Phys. Letters **25B**, 156 (1967).
[12] A. D. Krisch, Phys. Rev. **135**, B1456 (1964); *Lectures in Theoretical Physics* (University of Colorado Press, Boulder, Colo., 1966), Vol. IX.
[13] J. J. J. Kokkedee and L. Van Hove, Phys. Letters **25B**, 228 (1967).

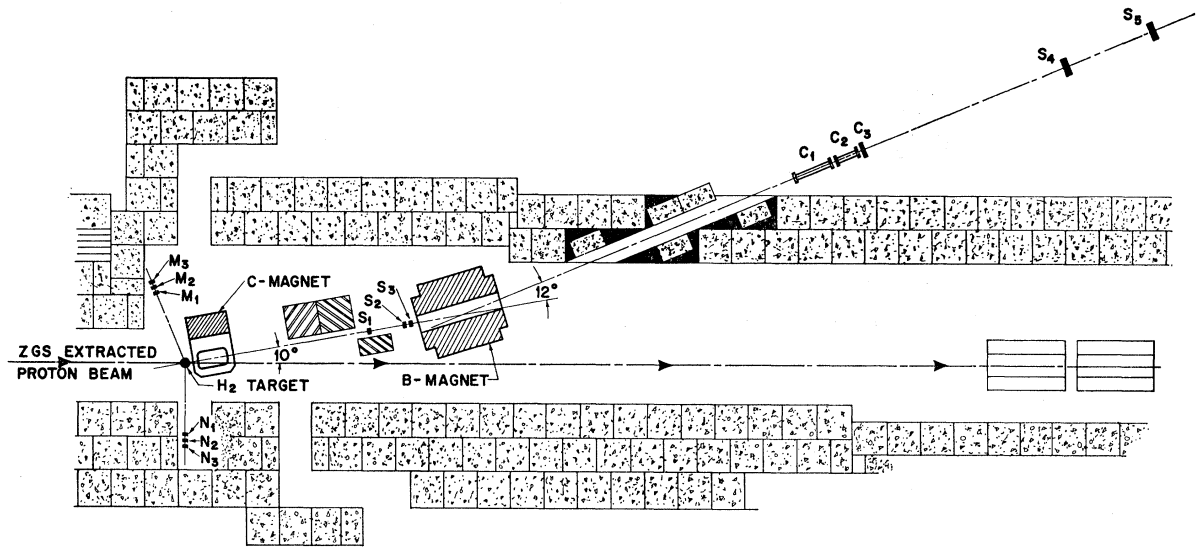

FIG. 2. Layout of the experiment. The incident protons come down the extracted beam and strike the hydrogen target. The produced particles are detected by the spectrometer.

uncertainty in the absolute value of the momentum of the beam was less than $\frac{1}{2}\%$.

The extracted proton beam was transported from the ZGS by a system consisting of two quadrupole doublets with a bending magnet between them. The beam was tuned by varying the current of this bending magnet. A triple scintillation counter telescope $B = B_1B_2B_3$ viewed a $\frac{1}{16}$-in.-thick Lucite flip target which was placed near the exit port of the ZGS. This target was upstream from all the beam-transport elements. Two other sets of monitor telescopes $M = M_1M_2M_3$ and $N = N_1N_2N_3$ viewed our H_2 target. The ratios M/B and N/B were maximized by varying the current in the beam-bending magnet and thus sweeping the beam across the target.

The quadrupoles were set to values determined from standard beam tuning computer programs. The focus at the H_2 target was then checked by varying the quadrupoles in an appropriate manner and observing a maximum in the N/B and M/B ratios. The beam was much less sensitive to variations in quadrupole currents than to variations in the bending-magnet current.

B. Hydrogen Target and Monitoring

The target in this experiment was a vertical 2-in.-diam. flask of liquid hydrogen. The flask window and vacuum window were, respectively, 0.003-in. and 0.005-in. Mylar. These windows gave rise to a target-empty effect of about 25–30%. There was also a target-empty effect of around 5% from the aluminum case of the hydrogen target. The total target-empty effect was determined experimentally for each measurement by taking runs with the flask purged of hydrogen.

The number of protons passing through the target was measured by the two monitor telescopes M and N. As shown in Fig. 2, these both viewed the target so that the number of counts in these monitors was proportional to the number of protons passing through the target. Two monitors were employed so that one could check that the ratio $N:M$ was constant. In fact, it never varied by more than 5% and the two numbers N and M were averaged to reduce systematic errors.

To obtain the ratio of protons to monitor counts, calibration runs were taken with aluminum and gold foils placed in the proton beam several feet upstream of the target. During each calibration run, the number of monitor counts was recorded. The number of protons which passed through the foil (and thus through the target) were determined by measuring the production of F^{18}, Na^{24}, and Tb^{149} in the foil. The production of

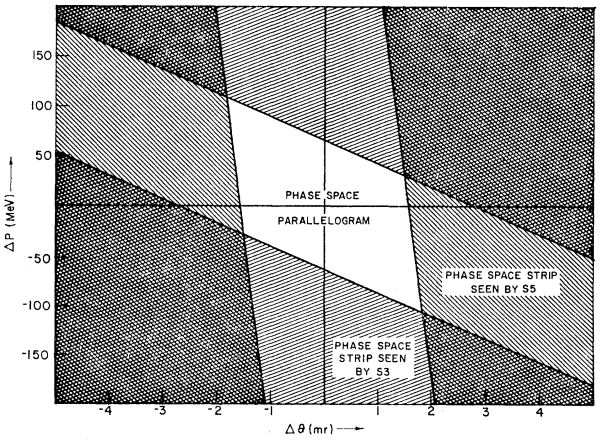

FIG. 3. Plot of the phase space $\Delta\theta\Delta P$ of the produced particles. The strips subtended by the S_3 and S_5 counters are shown. The intersection of these two strips is the $\Delta\theta\Delta P$ subtended by the spectrometer.

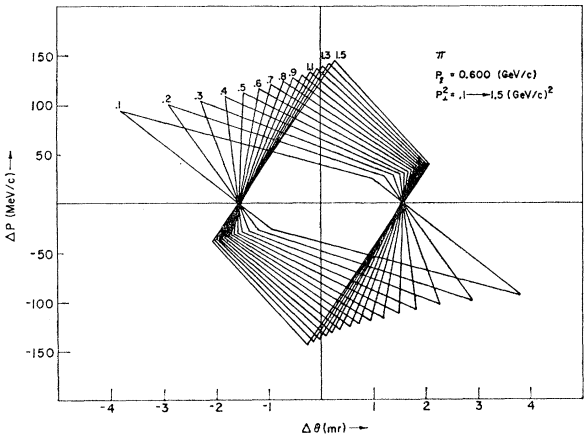

FIG. 4. Examples of the $\Delta\theta\Delta P$ parallelograms subtended by the spectrometer. This series of parallelograms corresponds to the series of $\pi^{\pm}$ measurements with $P_l=0.6$ GeV/c.

these elements was measured by doing a standard radiochemical analysis of the foils. The production cross sections of F^{18}, Na^{24}, and Tb^{149} are known to within $\pm 5\%$.[14] This introduced a normalization uncertainty but no point-to-point systematic error.

C. Spectrometer

The detection system for the produced particles was the single-arm spectrometer shown in Fig. 2. The spectrometer consisted of the C magnet for steering, the B magnet for momentum analysis, and a telescope of scintillation and Čerenkov counters to detect an identify the particles. Apart from the C magnet this spectrometer was essentially the same as the spectrometers that have been used in many "beam survey" experiments[1–5] in which the laboratory production angle $\theta_{\rm lab}$ was held fixed while the beam momentum $P_{\rm lab}$ was varied.

The telescope of three scintillation counters formed a coincidence $S_{123}=S_1S_2S_3$. The S_3 counter, which was $\frac{3}{4}$-in.$\times\frac{3}{4}$-in. and 270-in. from the target, nominally defined the solid angle of acceptance for the spectrometer ($\Delta\Omega_{\rm lab}\approx 10^{-5}$ sr).

The next element in the spectrometer was the B magnet which bent the particles through about 12° for momentum analysis. The counters S_4 and S_5 formed the coincidence $S_{45}=S_4S_5$ and the S_5 counter, which was 6 in.$\times$5 in. and 1100 in. from the target, nominally defined the momentum bite which was about $2\frac{1}{2}\%$ in the lab. The Čerenkov telescope identified the particles as pions, kaons, or antiprotons.

The extra component in our spectrometer was the C magnet placed very close to the H_2 target. This served as a steering magnet which compensated for the different laboratory angles of particles with different P_l and $P_\perp^2$ in the center-of-mass system. For example in the study of pions with $P_l=0.6$ GeV/c: When $P_\perp^2=0.5$ (GeV/c)^2, then $\theta_{\rm lab}$ was about 10° and the C magnet was essentially turned off. However, when $P_\perp^2=1.5$ (GeV/c)^2, then $\theta_{\rm lab}$ was about 14° and the C magnet bent in by 4° so that the particle still passed through the center of the S_3 counter. Similarly, when $P_\perp^2=0.1$ (GeV/c)^2, then $\theta_{\rm lab}$ was about 5° and the C magnet bent out by about 5° to put the particle through the center of S_3. The B magnet was then set to deflect the particle through the center of S_5.

The use of the C magnet eliminated the need to move the counters and magnets many times. It also resulted in the spectrometer being physically identical for all measurements, since only the two magnet currents were changed. Thus many possible sources of systematic error were eliminated. The C magnet effectively allowed us to do the experiment in the center-of-mass system.

The element of phase space subtended by the spectrometer at each value of $P_\perp^2$ and P_l was defined by the intersection of the two phase-space strips subtended by counters S_3 and S_5. The other counters were all overmatched. Figure 3 is a phase-space plot, with $\Delta\theta$ and ΔP as axes, showing typical phase-space strips subtended by counters S_3 and S_5. The strip subtended by S_3 makes a small angle with the ΔP axis. In the limit of the C magnet being turned off, this strip would be exactly parallel to the ΔP axis. The strip subtended by the S_5 counter makes an angle with the ΔP axis which was determined, to a large extent, by the 12° angle of bend in the B magnet. The area of $\Delta\theta\Delta P$ for which a particle will pass through both S_3 and S_5 is defined by the intersection of the two strips. As can be seen from Fig. 3, the region of interest is a parallelogram. Typical parallelograms of phase space for π mesons with $P_l=0.6$ GeV/c at the values of $P_\perp^2$ covered in the experiment are plotted in Fig. 4. The phase-space area was calculated from these parallelograms which

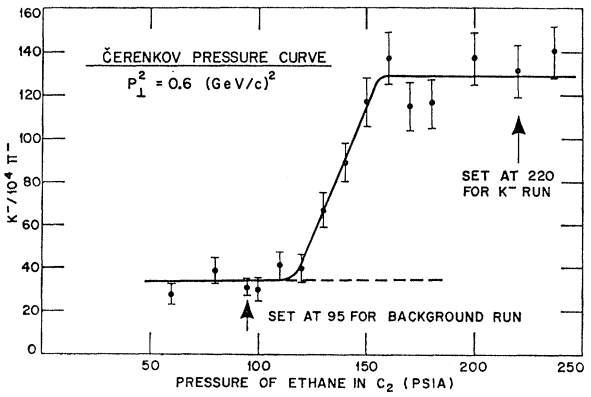

FIG. 5. Čerenkov pressure curve for K^- mesons. Notice the K-meson plateau and the plateau at lower pressure corresponding to unrejected π^- mesons.

[14] J. B. Cummings, J. Hudis, A. M. Poskanzer, and S. Kaufman, Phys. Rev. 128, 2392 (1962); J. B. Cummings, Ann. Rev. Nucl. Sci. 13, 261 (1963).

take into account the focusing by the two bending magnets.

The vertical aperture is defined by the vertical angle $\Delta\varphi$ subtended by counter S_3. The vertical size of S_5 was overmatched. The product of $\Delta\varphi$ with the area of the $\Delta\theta\Delta P$ parallelogram gives the subtended phase-space area $\Delta\Omega\Delta P$. The laboratory phase-space bite was typically $(\Delta\Omega\Delta P)_{\text{lab}}=1.5\times10^{-6}$ sr GeV/c, while the center-of-mass phase-space bite was typically $(\Delta\Omega\Delta P)_{\text{c.m.}}=5\times10^{-6}$ sr GeV/c.

The magnetic field integrals $\int\mathbf{B}\cdot d\mathbf{l}$ of the B and C magnets were measured by the ZGS staff,[15] using NMR, flip-coil, and floating-wire techniques. For this experiment the magnets were calibrated by NMR measurements. During the experiment the magnet currents were set by reading the voltage across a standard shunt with two digital voltmeters in parallel.

D. Čerenkov Counters

The Čerenkov telescope served to identify the particles as pions, kaons, or antiprotons. C_1 and C_2 were threshold Čerenkov counters filled with ethane gas, and C_3 was a scintillation counter used only to reduce accidentals. The C_2 counter was always run in coincidence while C_1 was run in anticoincidence to reject pions during the kaon runs and to reject pions and kaons during the antiproton runs. During the kaon runs, for example, the C_2 pressure was set high enough to trigger on pions and kaons but not on protons. The C_1 pressure was set to trigger on pions but not on kaons or protons. The appropriate ethane pressures for C_1 and C_2 were determined experimentally by running pressure curves. Typical pressure curves on C_2 for the K^-, K^+, and $\bar{p}$ runs are shown in Figs. 5–7. Such pressure curves were taken at several values of $P_\perp^2$ and P_l spanning our complete range of P_{lab}, to experimentally

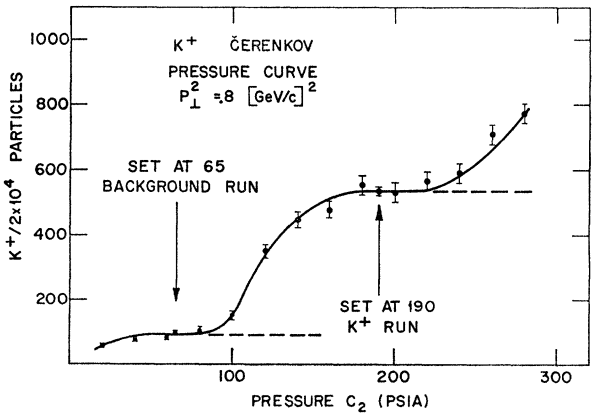

FIG. 6. Čerenkov pressure curve for K^+ mesons. Notice first the low-pressure plateau of unrejected π^+ meson, the K^+ plateau, and finally the sharp rise as we begin to detect protons.

[15] R. J. Lari, Argonne National Laboratory ANL-PAD Reports RJL-2, RJL-3, RJL-5, RJL-6 (unpublished).

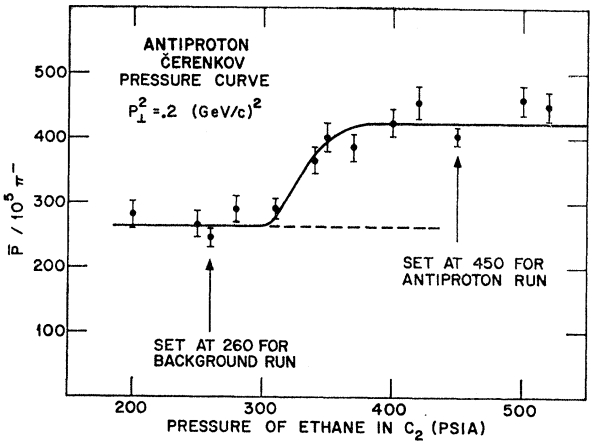

FIG. 7. Čerenkov pressure curve for antiprotons. Notice the low-pressure plateau of unrejected π^- and K^- mesons and then the antiproton plateau.

measure the threshold pressure as a function of the velocity of the kaons and antiprotons. These measurements agreed well with calculated threshold pressures.[16]

The Čerenkov rejection efficiency was only about 0.997, so it was necessary to make background runs in order to estimate the number of unrejected particles in the kaon and antiproton runs. In K^- runs, for example, this was done by running C_2 at a low pressure so that C_2 would not trigger on kaons but only on pions. Then any particles which triggered C_2 but not C_1, which was in anticoincidence, were pions which were not rejected by our system. This background contamination was estimated accurately by this low-pressure run as shown in Fig. 5. The background subtraction was always 25% or less for kaons but as much as 60% for the antiprotons.

The Čerenkov counters were similar in design except that C_1 was longer. A diagram of C_2 is shown in Fig. 8. The ethane was contained in a $\frac{1}{2}$-in.-thick aluminum tube of 5-in. i.d. The particles entered and exited from the tube through 0.1-in.-thick aluminum windows. Aluminized Mylar was wrapped around the inside of the tube for reflection. The particle path length in ethane for C_2 was 20 in., while for C_1 it was 38 in. A 56 UVP photomultiplier was optically coupled to a UVT Lucite light pipe shaped like a truncated cone. The Čerenkov light was reflected into the light guide by a thin aluminized Lucite mirror placed at an angle of 45° in the tube.

E. Counters and Electronics

The counters S_1, S_2, and S_3 were made up from $\frac{1}{2}$-in.-thick pieces of Pilot B scintillator of sizes 1-in. $\times1\frac{1}{4}$-in., 1-in.$\times$1-in., and $\frac{3}{4}$-in.$\times\frac{3}{4}$-in., respectively. Each scintillator was viewed by an RCA 7746 photo-

[16] W. Galbraith, *High Energy and Nuclear Physics Handbook* (Rutherford High Energy Laboratory, England, 1964), Sec. VI.

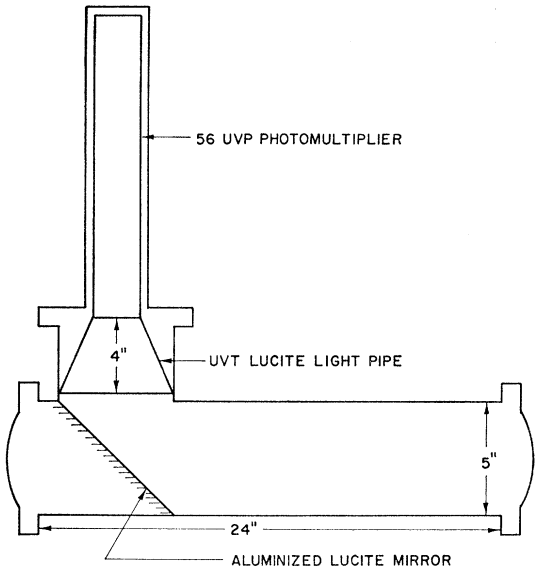

FIG. 8. Diagram of the threshold Čerenkov counters. Čerenkov light is created in the main tube, deflected by the 45° mirror into the lucite light guide which brings the light onto the cathode of the 56UVP photomultiplier tube.

multiplier tube via an air light guide. These counters were in a region of high background-particle intensities inside the extracted beam tunnel. Light guides of Lucite, or similar material, would have resulted in a large contribution to the singles rates in the counters due to Čerenkov radiation. The use of air light guides eliminated this effect. Counters S_4 and S_5 were constructed from $\frac{1}{2}$-in.-thick scintillator of dimensions 6 in.$\times$6 in. and 6 in.$\times$5 in., respectively. Their light guides were made from Lucite.

The logic system consisted of 100-Mc/sec Chronetics coincidence circuitry. A block diagram of the logic system is shown in Fig. 9. The outputs from the logic were displayed on 100-Mc/sec TSI scalers and recorded with a Polaroid camera. Important quantities were double scaled. The time-of-flight spectra were displayed on a 400-channel TMC pulse-height analyzer (PHA).

The three signals S_1, S_2, and S_3 came together to form the threefold coincidence S_{123}; similarly the signals S_4 and S_5 formed a twofold coincidence S_{45}. S_{123} and S_{45} were brought together to form the coincidence S_{fast}; this was a measure of the number of particles passing through the spectrometer. To identify the particles the C_1, C_2, and C_3 signals were fed together to form the coincidence C. For pions C_1 was switched out, while for antiprotons and kaons it was in anticoincidence. The resolving times of these circuits were about 5 nsec.

The S_{123}, S_{45}, and C signals formed a coincidence SC_{fast} if they arrived within 5 nsec of each other. The number of SC_{fast} events would be equal to the number of pions, kaons, or antiprotons detected by the spectrometer if there were no accidental or background events.

Two techniques were used to estimate the number of accidental coincidences. In the first, the output pulses from S_{123}, S_{45}, and C were stretched and formed the SC_{slow} coincidence with a resolving time of $\sim$30 nsec. Then the quantity $SC_{\text{slow}}-SC_{\text{fast}}$ was a measure of the accidentals since the resolving times were known. For instance, if SC_{slow} was equal to SC_{fast}, then there were no accidentals and all coincidences were true events. This technique was generally used as a monitor of the accidentals while running.

The second technique was more accurate and was used in correcting the data. The time of flight of the particles was measured between S_3 and S_5 by means of a time-to-amplitude converter (TAC). Stretched pulses from S_3 and S_5 were fed to the TAC which was triggered by every SC_{slow} pulse. The TAC gave out a pulse whose height in volts was proportional to the time overlap of the S_3 and S_5 pulses. This pulse was analyzed by the PHA and then stored in the appropriate channel of its memory. Thus the time-of-flight spectrum of the particles passing through the spectrometer was measured and then stored and displayed by the PHA. A typical time-of-flight spectrum is shown in Fig. 10. Each channel is about 0.4 nsec wide. The true events appear as a large peak about 1.5 nsec wide at half-maximum. The accidentals appear as a broad flat region about 30 nsec wide; the number under the peak can be accurately calculated and subtracted out. The subtraction varied between 2 and 20% with an uncertainty between 1 and 5%.

3. RESULTS

A. Corrections and Experimental Errors

There were a number of corrections made to the raw data before the cross sections were determined and

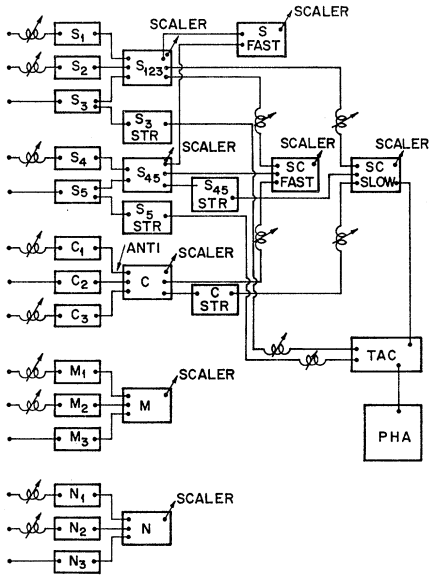

FIG. 9. Electronics block diagram for formation of SC_{slow} and SC_{fast} coincidences and for time-of-flight analysis.

several uncertainties were involved in this correction procedure.

The largest correction was the subtraction of the target-empty effect. As mentioned above this was a subtraction of about 30%. There was essentially no systematic error in this determination of the target-empty effect. This was because the effect was experimentally determined by taking target-empty runs with the flask purged of its hydrogen. However, before making the subtraction it was necessary to correct the target-full and target-empty raw data for both accidental events and for unrejected particles in the kaon and antiproton runs. The subtraction for accidental events was 1% for pions, 5–10% for kaons and 10–15% for antiprotons. The uncertainty in this subtraction varied between 0 and 5%. The subtraction for unrejected particles was less than 25% for the kaon runs and about 60% for the antiprotons. This was experimentally determined, with a systematic error of ~2%, by taking low-pressure runs as described in Sec. 2D.

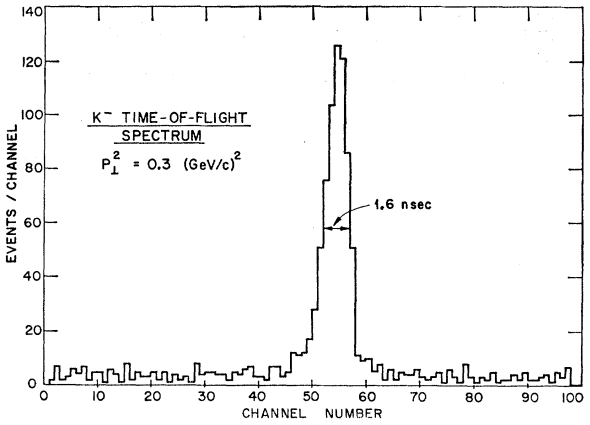

FIG. 10. Time-of-flight spectrum from the pulse-height analyzer. Number of coincidences is plotted against the time of flight between the S_3 and S_5 counters. Each channel is 0.4 nsec wide.

TABLE I. Center-of-mass production cross sections for the production of π^+ and π^- mesons in 12.5-GeV/c proton-proton collisions.

Particle	$P_1^{c.m.}$ (GeV/c)	$P_\perp^2$ (GeV/c)^2	$(\Delta\Omega\Delta P)_{c.m.}$ (10^{-6} sr GeV/c)	$(d^2\sigma/d\Omega dP)_{c.m.}$ [μb/sr (GeV/c)]	Error in $(d^2\sigma/d\Omega dP)_{c.m.}$ (±%)
π^-	0.6	0.1	5.89	1873	4.2
		0.2	5.91	1228	3.9
		0.3	5.95	781	3.9
		0.4	6.01	614	3.2
		0.5	6.08	410	3.3
		0.6	6.16	291	4.6
		0.7	6.24	199	4.2
		0.8	6.32	146	4.2
		0.9	6.40	108	4.6
		1.0	6.48	77.2	5
		1.1	6.56	53.0	6
		1.2	6.64	36.0	6
		1.3	6.72	25.3	6
		1.4	6.79	19.3	6
		1.5	6.87	13.6	6
π^-	0.4	0.1	4.11	2128	3.2
		0.2	4.16	1371	3.3
		0.3	4.25	915	4.6
		0.4	4.35	625	3.3
		0.5	4.46	444	4.6
		0.6	4.57	299	4.2
		0.7	4.68	183	5
		0.8	4.79	132	6
		0.9	4.89	90.9	5
		1.0	5.00	64.2	5
π^+	0.6	0.1	5.89	3628	3.0
		0.2	5.91	2444	3.0
		0.3	5.95	1760	3.0
		0.4	6.01	1278	3.1
		0.5	6.08	926	3.1
		0.6	6.16	666	3.1
		0.7	6.24	487	3.1
		0.8	6.32	353	3.5
		0.9	6.40	258	3.5
		1.0	6.48	189	3.6
		1.1	6.56	134	3.6
		1.2	6.64	98.1	3.6
		1.3	6.72	71.3	4.1
		1.4	6.79	51.7	4.6
		1.5	6.87	39.2	4.6

The total statistical errors were in the range 1–6% for pions, 3–25% for kaons, and as much as 50% for antiprotons. There were only a few points with the larger errors at the very high values of transverse momentum.

A correction was made for the nuclear interaction of the particles in the early components of the spectrometer. The correction was calculated to be 1.14 for pions, 1.15 for kaons, and 1.30 for antiprotons. There was a 2% uncertainty in this correction. There was also a correction for the decay of pions and kaons before reaching S_5, the last counter in the spectrometer. This correction varied between 1.09 and 1.28 for pions and between 1.93 and 5.8 for kaons. The uncertainty in this correction varied between 0 and 5%. The correction was calculated by using a Monte Carlo program which took into account the half-life of the particles, the path length, and the size of the S_5 counter.

No correction was made for multiple Coulomb scattering, because in-scattering is equal to out-scattering in a single-arm spectrometer with small $\Delta\Omega\Delta P$.

Since the magnets and counters were not moved throughout the experiment, there was no point-to-point systematic error due to misalignment of equipment. The only possible error was due to incorrect magnet currents in B and C. However, there was sufficient overmatching to allow for a 1% error in any magnetic field integral. Since the estimated uncertainty in the field integrals was $\frac{1}{2}$% no correction was made for this effect and we believe there was no error.

The most significant source of systematic error was in the determination of the incident proton flux. First there is an uncertainty in the spallation cross sections[14] used in the radiochemical analysis of the foils. This gave rise to a 5% normalization uncertainty. There was also an uncertainty in the calibration of the N and M monitor counters. This was primarily due to the fringe

TABLE II. Center-of-mass production cross sections for the production of K^+, K^-, and antiprotons in 12.5-GeV/c proton-proton collisions.

Particle	$P_l^{c.m.}$ (GeV/c)	$P_\perp^2$ (GeV/c)^2	$(\Delta\Omega\Delta P)_{c.m.}$ (10^{-6} sr GeV/c)	$(d^2\sigma/d\Omega dP)_{c.m.}$ [μb/sr (GeV/c)]	Error in $(d^2\sigma/d\Omega dP)_{c.m.}$ (±%)
K^-	0.6	0.1	8.72	43.7	7
		0.2	8.28	23.6	9
		0.3	8.02	16.0	9
		0.4	7.85	11.3	10
		0.5	7.74	8.61	10
		0.6	7.68	5.32	13
		0.7	7.64	3.74	13
		0.8	7.63	2.31	14
		0.9	7.62	1.31	15
		1.0	7.63	1.18	16
		1.1	7.65	1.06	16
		1.2	7.68	0.83	18
		1.3	7.71	0.54	26
		1.4	7.74	0.52	24
		1.5	7.78	0.26	28
K^+	0.6	0.1	8.72	262	6
		0.2	8.28	227	6
		0.3	8.02	167	6
		0.4	7.85	135	6
		0.5	7.74	105	6
		0.6	7.68	74.1	6
		0.7	7.64	56.6	6
		0.8	7.63	44.5	6
		0.9	7.62	31.2	8
		1.0	7.63	25.7	8
		1.1	7.65	18.1	7
		1.2	7.68	15.1	8
		1.3	7.71	11.1	9
		1.4	7.74	8.28	8
		1.5	7.78	7.05	7
$\bar{P}$	0.6	0.2	15.66	0.63	19
		0.3	14.40	0.44	19
		0.4	13.49	0.16	37
		0.5	12.82	0.11	60

field of the C magnet which was not zero between the H_2 target and the N and M monitors. The effect of changes in the C-magnet field on the N and M counters was determined experimentally; the calibration changed as much as 5% with an uncertainty of 2%.

B. Calculation of Cross Sections

The differential production cross section in the center-of-mass system was calculated from the formula

$$\frac{d^2\sigma}{d\Omega dP}=\frac{\text{Events}}{I_0(N_0\rho t)\Delta\Omega\Delta P}, \quad (1)$$

where I_0 is the number of incident protons as measured by the monitors, N_0 is Avogadro's number 6.02×10^{23}, ρ is the density of liquid hydrogen taken as 0.07 g/cc, t is the target length, taken as 5.08 cm, and $\Delta\Omega\Delta P$ is the center-of-mass phase-space volume.

The calculated cross sections and errors for $\pi^\pm$, $K^\pm$, and $\bar{p}$ are tabulated in Tables I–III against the c.m. variables P_l and $P_\perp^2$.

The errors include both systematic and statistical errors which have been added in quadrature. Not included is the normalization uncertainty from the foil calibrations which may shift all points up or down by 5%.

4. DISCUSSION

As mentioned in the Introduction, the main purpose of this experiment was to begin a systematic study of the dependence of the differential production cross section on center-of-mass variables. Previous experiments[1–5,17] of the "beam survey" type studied the dependence of $d^2\sigma/d\Omega dP$ on laboratory variables; normally θ_{lab} was held fixed while P_{lab} was varied. On the basis of the data obtained from these experiments, several authors[6–8,18–20]

TABLE III. Center-of-mass production cross sections for the production of $\pi^\pm$ and $K^\pm$ mesons in 12.5-GeV/c proton-proton collisions.

Particle	$P_l^{c.m.}$ (GeV/c)	$P_\perp^2$ (GeV/c)^2	$(\Delta\Omega\Delta P)_{c.m.}$ (10^{-6} sr GeV/c)	$(d^2\sigma/d\Omega dP)_{c.m.}$ [μb/sr (GeV/c)]	Error in $(d^2\sigma/d\Omega dP)_{c.m.}$ (±%)
π^-	0.1	0.4	2.27	197	7
	0.2		2.88	382	5
	0.3		3.59	567	3.9
	0.4		4.35	625	3.3
	0.5		5.17	654	3.2
	0.6		6.01	614	3.2
	0.7		6.89	515	3.6
	0.8		7.78	478	3.6
	0.9		8.68	396	3.6
	1.0		9.59	339	3.6
π^+	0.1	0.4	2.27	234	5
	0.2		2.88	607	3.6
	0.3		3.59	1002	3.4
	0.4		4.35	1302	3.2
	0.5		5.17	1325	3.2
	0.6		6.01	1278	3.2
	0.7		6.89	1216	3.2
	0.8		7.78	1091	3.2
	0.9		8.68	1025	3.2
	1.0		9.59	937	3.2
K^-	0.1	0.4	3.79	8.1	18
	0.2		4.60	11.8	11
	0.3		5.42	12.5	11
	0.4		6.24	13.8	10
	0.5		7.05	10.5	10
	0.6		7.85	11.3	13
	0.7		8.66	7.3	11
	0.8		9.47	7.2	10
	0.9		10.29	5.2	13
K^+	0.0	0.4	3.03	21.4	18
	0.1		3.79	38.0	10
	0.2		4.60	73.3	7
	0.3		5.42	85.3	7
	0.4		6.24	104	7
	0.5		7.05	131	7
	0.6		7.85	135	7
	0.7		8.66	131	7
	0.8		9.47	113	7
	0.9		10.29	120	7

[17] J. V. Allaby *et al.*, CERN Report NP/Int 66-2, 1966 (unpublished).

[18] J. R. Sanford and C. L. Wang, Brookhaven National Laboratory AGS Internal Report, 1967 (unpublished).

[19] P. Haberler, CERN Report MPS/Int 63-23, 1964 (unpublished).

[20] G. von Dardel, CERN Report NP 62-17, 1962 (unpublished).

have proposed parametrizations of the data. The simplest and best-known parametrization was that of Cocconi, Koester, and Perkins,[6] which suggested that $d^2\sigma/d\Omega dP$ was an exponential in the transverse momentum. Essentially all of these fits were consistent with the experiments. However, none of these experiments gave a very stringent test of these fits; their main purpose was to aid in the design of beams of secondary particles, not to obtain information about the nature of strong interactions.

The present experiment[9] was planned to study the dependence of $d^2\sigma/d\Omega dP$ on center-of-mass variables, in the hope that the cross section would have its simplest form in this Lorentz frame. As we shall see later it appears that there is another Lorentz frame, the "fireball" rest frame, in which things appear to be even simpler. Nevertheless a very significant improvement was obtained by choosing the center-of-mass system over the laboratory system.

Recall that this experiment consisted of measuring the probability ($d^2\sigma/d\Omega dP$) that a particle was emitted in the phase-space region $\Delta\Omega\Delta P$ when two protons passed by each other. Great care was taken to have no knowledge of what other particles emerged from the interaction, for obtaining such knowledge would be equivalent to measuring a different type of cross section, such as $d^4\sigma/d\Omega_1 d\Omega_2 dP_1 dP_2$. Avoiding any such knowledge was equivalent to summing over all channels in which the particle of interest was emitted in $\Delta\Omega\Delta P$. For example, in studying the process

$$p+p\rightarrow\pi^+ + \text{anything}, \tag{2}$$

we have summed over the following channels in additon to many others.

$$\begin{aligned} &p+p\rightarrow p+n+\pi^+,\\ &p+p\rightarrow p+p+\pi^+ +\pi^-,\\ &p+p\rightarrow p+n+\pi^+ +\pi^0. \end{aligned} \tag{3}$$

In this type of measurement there are two[21] independent variables in addition to the energy of the incident particles. These two variables describe the magnitude and direction of the momentum of the produced particle. For these two variables we have chosen the transverse momentum ($P_\perp$) and the longitudinal momentum (P_l) of the produced particle in the center-of-mass system. These variables are frequently used in the study of cosmic-ray jets. In the present experiment a series of measurements consisted of holding one of these two variables at a fixed value while varying the other variable over some range. The range covered is shown in Fig. 1. By taking cuts in this way we were able to independently measure the dependence of $d^2\sigma/d\Omega dP$ on $P_\perp$ and $P_l^{\text{c.m.}}$.

In Fig. 11 we have plotted the measurements in which $P_l^{\text{c.m.}}$ was held fixed and $P_\perp^2$ was varied over the range $0.1\rightarrow 1.5$ (GeV/c)^2. For the majority of points $P_l^{\text{c.m.}}$ was held at 0.6 GeV/c, but for one series of π^- measurement $P_l^{\text{c.m.}}$ was equal to 0.4 GeV/c. These results are also listed in Tables I and II, and cover the production of π^+, π^-, K^+, K^-, and antiprotons. In Fig. 11 we have plotted $d^2\sigma/d\Omega dP$ against $P_\perp^2$ on semilog paper. There are several very interesting results from this series of measurements.

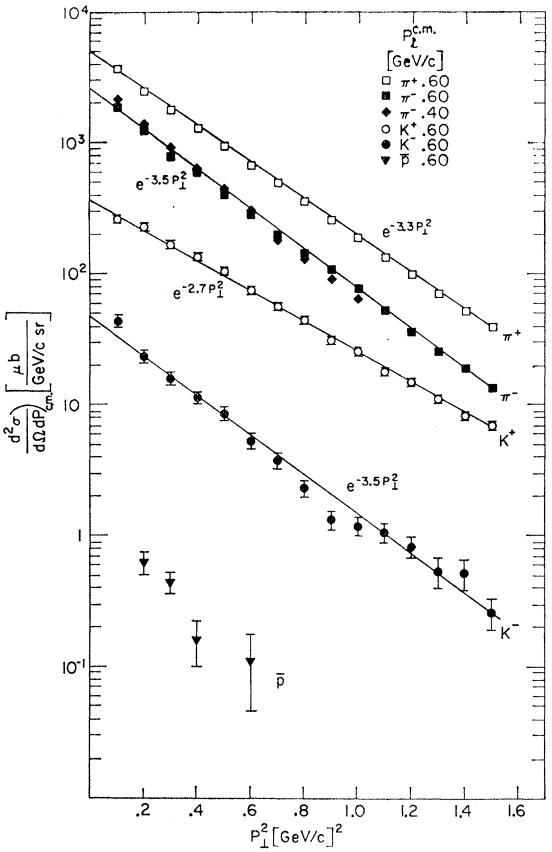

FIG. 11. Plot of $d^2\sigma/d\Omega dP$ against $P_\perp^2$ for $P_l^{\text{c.m.}}$ held fixed. The production cross sections for π^+, π^-, K^+, K^-, and antiprotons are shown. The lines are straight-line fits to the data.

A. Gaussian Dependence on $P_\perp$

First notice that $d^2\sigma/d\Omega dP$ appears to be a Gaussian in the transverse momentum over the entire range of measurements:

$$d^2\Omega/d\Omega dP\sim\exp(-AP_\perp^2). \tag{4}$$

This appears to be true for the production of all five types of particles. However, the uniqueness of the Gaussian dependence on $P_\perp$ varies considerably for the different particles. The best one can say about the large-error $\bar{p}$ measurements is that they are consistent with a Gaussian. For the K^- measurements a Gaussian appears to be the best fit. There is strong evidence for a

[21] There is also a third variable φ, the azimuthal angle. However, in an experiment with an unpolarized target and unpolarized beam, the cross section cannot depend on φ.

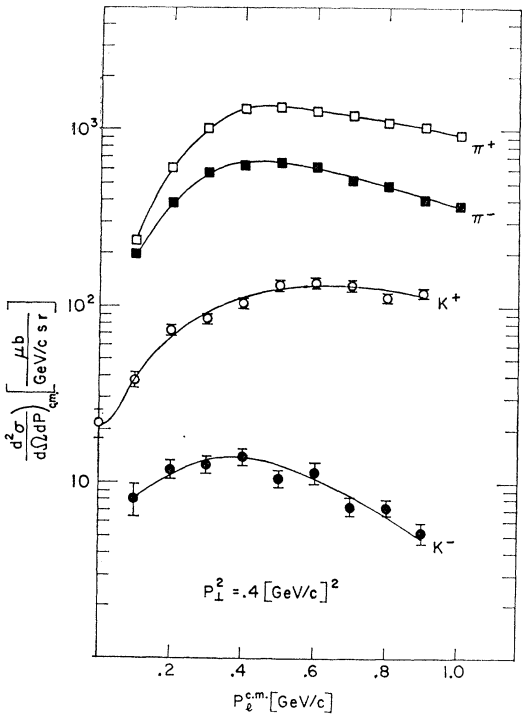

FIG. 12. Plot of $d^2\sigma/d\Omega dP$ against P_l for $P_\perp{}^2$ held fixed. The cross sections for π^+, π^-, K^+, and K^- production are shown. The lines are freehand fits to the data.

Gaussian in the K^+ measurements and in the case of the π^+ and π^- measurements the Gaussian dependence seems absolutely certain. In the region covered there is no question about the straight-line fit. This Gaussian dependence is in disagreement with the widely accepted Cocconi, Koester, and Perkins[6] parametrization which predicted an exponential dependence on $P_\perp$.

The reason for this Gaussian dependence is not at all clear. It should be noted that a recent precise experiment[10] has also shown the proton-proton elastic scattering cross section to be Gaussian in something like the transverse momentum transfer. A possible explanation of this Gaussian dependence has recently been proposed.[22] It was suggested that the existence of a large number of independent channels leads to a Gaussian through the central limit theorem of mathematical statistics. This behavior is independent of the dynamics of the individual channels. This idea must still be considered very speculative.

B. Equal Slopes in $P_\perp{}^2$ Plot

Notice that except for the K^+ spectrum all cross sections are consistent with a slope of $A \approx 3.5$ $(\mathrm{GeV}/c)^2$ in Fig. 11:

$$d^2\sigma/d\Omega dP \sim \exp(-3.5P_\perp{}^2). \tag{5}$$

[22] A. D. Krisch, J. P. Krisch, 1967 Heidelberg International Conference on High-Energy Physics (unpublished).

This slope is some measure of the "size" of the region from which the particles come. The equality of the π^+, π^-, K^-, and $\bar{p}$ slopes seems to imply that these particles all come from regions of the same size.

This point was part of the original impetus for this experiment; an attempt to see if different particles came from different parts of the proton. Recently it has been shown[10,11] that in some sense the proton-proton elastic interaction has three distinct regions. One of us speculated[12] that these three regions were the diffraction scattering associated with three different types of inelastic interactions: pion, kaon, and antibaryon production.

A relation between these two types of experiments comes from noticing that the production probability density, ρ, for producing particles in high-energy collisions depends on two variables R and r. The quantity R is the distance between the two incoming particles at the time of interaction, while r is the distance from one of the incident particles to the point at which the produced particle is created. The distance r is the canonically conjugate variable to the momentum of the produced particle. Similarly, through unitarity we have that R is canonically conjugate to the momentum of the elastically scattered particle. Thus in an elastic scattering experiment one measures the R dependence of $\rho(R,r)$ while in this production experiment we measured the r dependence.

The speculation was that the three regions in elastic scattering could be associated with the π, K, and $\bar{p}$ production. To study the significance of this idea we assume that $\rho(R,r)$ is factorable:

$$\rho(R,r)=\rho'(R)\rho''(r). \tag{6}$$

Then the speculation is equivalent to saying that the functional forms of $\rho_\pi'(R)$, $\rho_K'(R)$, and $\rho_{\bar{p}}'(R)$ are different in a way which would give the three different slopes in elastic scattering. In fact the K and $\bar{p}$ regions must be progressively smaller. This seems sensible because of the heavier quanta involved.

This experiment would have tested this model if it had turned out that ρ' and ρ'' had identical functional forms—that is, if

$$\rho'(X)\equiv\rho''(X) \tag{7}$$

for the π, K, and $\bar{p}$ processes. Then the $K^\pm$ and $\bar{p}$ dependence in Fig. 11 might have been progressively flatter than the π dependence. Clearly this is not true experimentally. There are two possible conclusions.

(a) The entire idea is wrong. The three regions in elastic scattering are not associated with pion, kaon, and antiproton production.

(b) The central idea is correct and the three regions are associated with π, K, and $\bar{p}$ production. However, Eq. (7) is wrong and all $\rho''(r)$ are identical, so that

$$\rho(R,r)=[\rho'_\pi(R)+\rho'_K(R)+\rho'_{\bar{p}}(R)]\rho''(r). \tag{8}$$

At the present time, there is no way to distinguish between these two conclusions. Perhaps some new experiment can be devised to test the validity of this idea.

There are two other interesting aspects to the slopes. First it is clear that the K^+ slope is ~ 2.7 $(\mathrm{GeV}/c)^{-2}$ while all the other slopes are about 3.5. The reason for this is not at all clear.

The other interesting fact is that while these production cross sections drop off with a slope of about 3.5 $(\mathrm{GeV}/c)^{-2}$ all known elastic cross sections decrease with a slope of 8 to 10 $(\mathrm{GeV}/c)^{-2}$ in the small-angle region. Again the reason for this is not at all clear. However, it could have some relation to the fact that the slope of the second region in p-p elastic scattering is 3.3 $(\mathrm{GeV}/c)^{-2}$.[10]

C. Production of Fireballs

The other part of the experiment consisted of holding $P_\perp^2$ fixed at 0.4 $(\mathrm{GeV}/c)^2$ while varying $P_l^{c.m.}$ over the range 0.0 to 1.0 GeV/c. This was done for π^+, π^-, K^+, and K^- particles and the results are tabulated in Table III. These results are plotted in Fig. 12 where $d^2\sigma/d\Omega dP$ is plotted against $P_l^{c.m.}$, the longitudinal momentum of the produced particle in the center-of-mass system.

TABLE IV. The values of the cross sections and momenta transformed into the fireball rest frame which is defined to be moving with $\beta=0.54$ with respect to the center of mass.

Particle	P_l^F (GeV/c)	$(P_l^F)^2$ $(\mathrm{GeV}/c)^2$	$P_\perp^2$ $(\mathrm{GeV}/c)^2$	$(d^2\sigma/d\Omega dP)_{\text{fireball}}$ [μb/(GeV/c) sr]	Error (±%)
π^-	−0.302	0.091	0.4	216	7
	−0.197	0.039		382	5
	−0.102	0.010		517	3.9
	−0.013	0.000		525	3.3
	0.069	0.005		512	3.2
	0.146	0.021		453	3.2
	0.220	0.048		362	3.6
	0.290	0.084		323	3.6
	0.358	0.128		259	3.6
	0.424	0.180		216	3.6
π^+	−0.302	0.091	0.4	257	5
	−0.197	0.039		606	3.6
	−0.102	0.010		914	3.4
	−0.013	0.000		1093	3.2
	−0.069	0.005		1036	3.2
	0.146	0.021		942	3.2
	0.220	0.048		854	3.2
	0.290	0.084		737	3.2
	0.358	0.128		670	3.2
	0.424	0.180		597	3.2
K^-	−0.400	0.160	0.4	10.0	18
	−0.293	0.086		12.6	11
	−0.193	0.037		11.6	11
	−0.100	0.010		11.2	10
	−0.013	0.000		7.6	10
	0.070	0.005		7.5	13
	0.149	0.022		4.5	11
	0.224	0.050		4.2	10
	0.296	0.088		2.9	13
K^+	−0.515	0.265	0.4	29.9	18
	−0.400	0.160		46.8	10
	−0.293	0.086		78.4	7
	−0.193	0.037		79.0	7
	−0.100	0.010		84.4	7
	−0.013	0.000		95.0	7
	0.070	0.005		89.5	7
	0.149	0.022		81.1	7
	0.224	0.050		66.5	7
	0.296	0.088		68.2	7

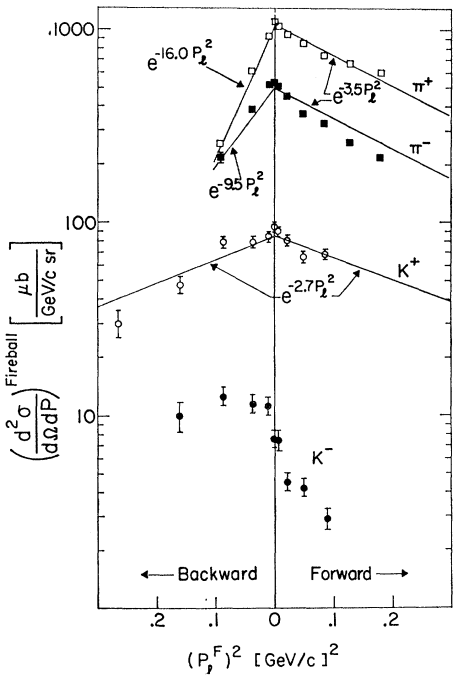

FIG. 13. Plot of $d^2\sigma/d\Omega dP$ against P_l^2 in the fireball rest frame. $P_\perp^2$ is held fixed at 0.4 $(\mathrm{GeV}/c)^2$. The cross sections for π^+, π^-, K^+, and K^- production are shown. The forward and backward direction are also indicated. This fireball rest frame is moving with $\beta=0.54$ with respect to the center of mass.

The most striking feature of Fig. 12 is that the cross sections are not maximum at $P_l^{c.m.}=0$. This is in direct contradiction to the statistical model.[23] The most fundamental idea of the statistical model is that the two incident particles stick together in some way to form one object, which then emits particles. This would result in the maximum number of particles being at rest in the center-of-mass system, giving a peak at $P_l^{c.m.}=0$.

Instead the cross sections all seem to peak at a forward value of $P_l^{c.m.}$ of about 0.5 GeV/c and by symmetry at a backward value of −0.5 GeV/c. This indicates that essentially all of the produced particles tend to come out in a fast cloud or "fireball" following one of the two baryons. Thus it appears that the two baryons act as centers from which the particles are emitted. A two-fireball model was suggested long ago in connection with high-energy cosmic-ray events.

In addition to showing that these two clouds or fireballs exist we can use the experimental results to determine some of the properties of these fireballs. We

[23] G. Fast and R. Hagedorn, Nuovo Cimento **27**, 203 (1963); G. Fast, R. Hagedorn, and L. W. Jones, *ibid.* **27**, 856 (1963).

can determine the mass of the fireball and the shape of the production cross section in the fireball rest frame. Notice from Fig. 12 that in the center-of-mass frame the shape is not very simple.

We can determine the mass by searching for a Lorentz frame in which $d^2\sigma/d\Omega dP$ peaks at zero longitudinal momentum. In fact we define the fireball rest frame to be that frame in which the cross section is maximum at $P_l=0$. By searching we found that this occurred for the Lorentz frame which is moving with $\beta=0.54$ with respect to the center of mass. We have transformed the cross sections and momenta into this fireball rest frame using the following transformations:

$$\begin{aligned} P_\perp{}^F &= P_\perp{}^{\text{c.m.}}, \\ P_l{}^F &= \gamma(P_l{}^{\text{c.m.}}-\beta E^{\text{c.m.}}), \\ \left.\frac{d^2\sigma}{d\Omega dP}\right|_F &= \frac{E_{\text{c.m.}}P_F{}^2}{E_F P_{\text{c.m.}}{}^2}\left.\frac{d^2\sigma}{d\Omega dP}\right|_{\text{c.m.}}. \end{aligned} \tag{9}$$

The transformed quantities are tabulated in Table IV and plotted in Fig. 13, where we have plotted $d^2\sigma/d\Omega dP$ against $(P_l{}^F)^2$. We can see that in this frame the cross section peaks at $P_l{}^F=0$, for π^+, π^-, and K^+ production. It does not peak at zero for K^- production.

Thus each "fireball" is moving with a velocity of $\beta=0.54$ with respect to the center of mass. The total energy of each fireball is $\frac{1}{2}$ of the total center-of-mass energy, if we assume that each fireball contains a baryon.

$$E_F=\tfrac{1}{2}W=\tfrac{1}{2}S^{1/2}=2.51 \text{ GeV}. \tag{10}$$

Then we recall that the mass and energy are related by

$$E_F=M_F/(1-\beta^2)^{1/2}. \tag{11}$$

This tells us that the fireball mass is

$$M_F=2.51[1-(0.54)^2]^{1/2}\approx 2100\pm 30 \text{ MeV}. \tag{12}$$

Next notice that for K^- production $d^2\sigma/d\Omega dP$ does not peak at $P_l=0$ in the $\beta=0.54$ frame. This indicates that K^- mesons tend to come from a cloud or fireball moving with a different velocity. Because of large errors it is difficult to get a very precise answer, but it appears that the K^- cross section peaks at $P_l=0$ in a frame moving with $\beta=0.4$ with respect to the center of mass. This indicates that K^- mesons come from a heavier fireball with a mass of

$$M_F{}^{K^-}\approx 2.51[1-(0.4)^2]^{1/2}\approx 2300\pm 30 \text{ MeV}. \tag{13}$$

Qualitatively this seems fairly sensible since a K^- can only be produced along with a K^+ and this pair production requires more energy than single K^+ or $\pi^\pm$ production.

Finally we can study the behavior of $d^2\sigma/d\Omega dP$ in the fireball rest frame for $\pi^\pm$ and K^+ production. We see from Fig. 13 that straight-line fits are not unreasonable in this frame. Thus the behavior in the fireball rest frame appears Gaussian in P_l as well as in $P_\perp$[24]:

$$(d^2\sigma/d\Omega dP)^F\sim\exp[-(AP_\perp{}^2+BP_l{}^2)]. \tag{14}$$

Moreover, in the forward direction the slope appears to differ only slightly from the 3.5 $(\text{GeV}/c)^{-2}$ slope of the $P_\perp{}^2$ distribution. However, for π^+ and π^- the backward $P_l{}^2$ slope is much steeper:

$$B^{\text{backward}}\approx 9.5\rightarrow 16 \text{ } (\text{GeV}/c)^{-2}. \tag{15}$$

Thus for $\pi^\pm$ production the cross section is Gaussian and is isotropic along the forward three axes but flattened along the backward axis. For K^+ production, all slopes seem equal to about 2.7 $(\text{GeV}/c)^{-2}$ so that we can write

$$d^2\sigma/d\Omega dP\sim\exp(-2.7P_F{}^2),$$

where P_F is the momentum of the K^+ in the fireball rest frame. The reason that K^+ production is isotropic while $\pi^\pm$ production is only partially isotropic is not at all clear.

Thus we have evidence that mesons are emitted from fireballs moving along with the baryons. Moreover, in the fireball rest frame $d^2\sigma/d\Omega dP$ appears Gaussian and at least partially isotropic.

ACKNOWLEDGMENTS

We would like to thank the entire ZGS staff for their help and encouragement during the entire experiment. We also thank Dr. E. Steinberg and the radio chemistry group for their assistance. We are grateful to Professor D. I. Meyer and Professor M. H. Ross for their helpful comments.

[24] In the fireball rest frame P_l is not constant during the series in which $P_\perp{}^2$ is varied from 0.1 to 1.5 $(\text{GeV}/c)^2$. However, it only changes slightly. This slight variation is responsible for the slight difference in slope of the two π^- runs in Fig. 11.